Chemical Geology, 69 (1988) 245–265
Elsevier Science Publishers B.V., Amsterdam — Printed in The Netherlands

[3]

GEOCHEMISTRY OF THE MERCUR GOLD DEPOSIT (UTAH, U.S.A.)

PAUL W. JEWELL* and W.T. PARRY

Department of Geology and Geophysics, University of Utah, Salt Lake City, UT 84112 (U.S.A.)

(Received April 1, 1987; revised and accepted January 19, 1988)

Abstract

Jewell, P.W. and Parry, W.T., 1988. Geochemistry of the Mercur gold deposit (Utah, U.S.A.). Chem. Geol., 69: 245–265.

The Mercur gold deposits of west-central Utah are disseminated "Carlin-type" deposits which are hosted by the upper portion of the Topliff Member of the Mississippian Great Blue Limestone. Strata-bound alteration and mineralization are related to sedimentary lithologies over a 60–80-m section of the Topliff Member. Hydrothermal alteration at Mercur can be separated into replacement and vein alteration assemblages. Two replacement assemblages are recognized. Jasperoid facies consists of replacement of massive limestone by silica and minor sericite and kaolinite. Argillic-facies alteration is characterized by decarbonation of silty limestones. Fluids which formed the argillic facies became progressively more reduced and acidic through reaction with carbonaceous argillaceous pyritiferous limestones. Three vein assemblages are recognized at Mercur: (1) pyrite–orpiment–organics ± marcasite; (2) calcite–realgar; and (3) halloysite–barite–calcite. Considerable temporal and spatial overlap exists among all hydrothermal assemblages. Varying degrees of Au mineralization are associated with most styles of alteration.

Fluid-inclusion studies show that jasperoid-facies rocks were formed at temperatures of 220–270 °C, hydrothermal calcite at 150–190 °C and barite at 150–300 °C. Salinities throughout the paragenesis remained relatively constant at 5–8 eq. wt.% NaCl.

A geochemical model based on fluid-inclusion data, microprobe data and mineral solubilities allows constraints to be placed on the chemical characteristics of the Mercur ore-forming fluids. Jasperoid-facies rocks were formed by fluids at pH > 3.6, $p_{CO_2} < 115$ bar, and $\log f_{O_2} > -34$ to -32. The argillic facies–vein assemblages were formed at a pH of ~4.0, p_{CO_2} of ~100 bar, $\log f_{O_2}$ of -40.4 to -39.6 and $\log f_{H_2S}$ of -3.1 to -2.7. The available data indicate ore-forming solutions are near a Au solubility minimum but do not allow an exact determination of the mechanism of Au deposition.

1. Introduction

Since the 1960's, gold deposits hosted by sedimentary rocks have become economically important to the mining industry of the western U.S.A. These ore deposits are collectively known as Carlin-type deposits after the Carlin mine in north-central Nevada. Carlin-type deposits are characterized by carbonate or silty carbonate host rocks, the introduction of quartz, pyrite, and/or barite, anomalous amounts of As, Sb, Hg and Tl, and Au which is only μm in size. Complete silicification of the host carbonates into jasperoids is a common feature of these de-

**Present address*: Department of Geological and Geophysical Sciences, Princeton University, Princeton, NJ 08544, U.S.A.

0009-2541/88/$03.50

posits, although other alteration styles such simple decarbonation, intense veining, introduction of carbonaceous material and acid–sulfate alteration are also typical (Bagby and Berger, 1985). Au mineralization is associated with some or all of these alteration styles, although the exact paragenesis of Au is not known in any Carlin-type deposit.

The Mercur Au deposits of west-central Utah are classified as Carlin-type deposits, although they have been mined intermittently since the early 1900's. The Mercur district is located ~90 km SW of Salt Lake City in the Oquirrh Mountains, a typical north–south-trending range of the Basin and Range province (Fig. 1A).

In spite of their economic importance, very few detailed geologic studies of Carlin-type deposits exist. With the exception of Carlin itself (Radtke et al., 1980; Radtke, 1985) there is virtually no comprehensive study of the hydrothermal fluid chemistry. This paper presents an integrated geochemical and fluid-inclusion study of the hydrothermal alteration of the Mercur deposit with the goal of defining the relevant chemical parameters of the hydrothermal fluids and by inference, the nature of the Au deposition.

2. Geology and mineral assemblages

2.1. General geology

The Mercur gold deposits are hosted by the Upper Mississippian Great Blue Limestone. This formation is part of a thick Paleozoic carbonate and clastic sedimentary section which outcrops in west-central Utah (Gilluly, 1932). The Great Blue Limestone is separated into three members. From upper to lower these are the Upper Great Blue Member, the Long Trail Shale Member and the Topliff Member (Fig. 1A). The upper 60–80 m of the Topliff Member are host to most of the Mercur hydrothermal alteration and Au mineralization.

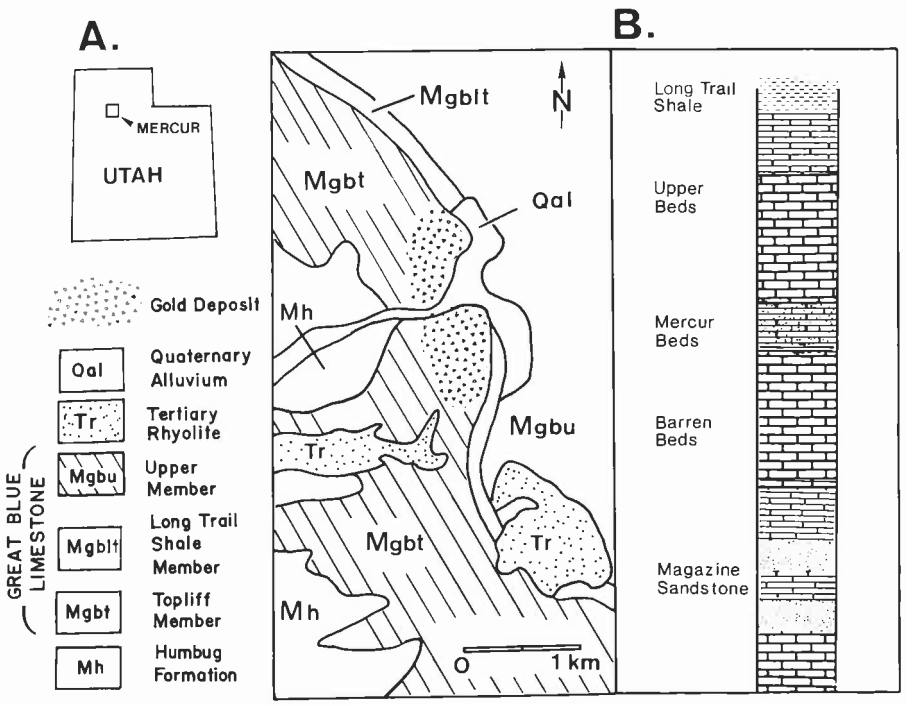

Fig. 1. A. Generalized geology of the southwestern portion of the Oquirrh Mountains, Utah (after Guilly, 1932). B. Generalized stratigraphy of the upper Topliff Member in the vicinity of the Mercur ore bodies.

The upper portion of the Topliff Member has distinct lithologies which appear to control the style of hydrothermal alteration (Fig. 1B). Approximately 60 m below the Topliff–Long Trail contact is 12–15 m of sandstone and limey sandstone known as the Magazine Sandstone. Unaltered massive limestone below the Magazine Sandstone shows localized karstification. This would appear to indicate that a groundwater system was active in the Magazine Sandstone prior to hydrothermal alteration.

Approximately 30–40 m below the Topliff–Long Trail contact is an 8-m-thick sequence of thinly bedded limestones and silty limestones known as the Mercur Beds. Limestones between the Long Trail Shale and the Mercur Beds are known as the Upper Beds. Limestone between the Mercur Beds and the Magazine Sandstone are known as the Barren Beds (Fig. 1B). Both Upper and Barren Beds are more massive and less porous than the Mercur Beds, Magazine Sandstone, or underlying limestones where they have undergone karstification.

X-ray diffraction (XRD) analyses of unaltered limestones and silty limestones show a relatively simple mineralogy of calcite with lesser amounts of quartz, illite and kaolinite. Minor pyrite and organic matter are present in varying amounts.

2.2. Hydrothermal alteration

Alteration at Mercur are divided into mineral assemblages which replace the host limestones and mineral assemblages which occur as veins. Considerable spatial and temporal overlap exists between all assemblages (Fig. 2).

The replacement assemblage can be separated into an early jasperoid facies and contemporaneous to somewhat later argillic facies. Jasperoid-facies rocks are common in the Magazine Sandstone and a 5–20-m-thick zone below the Magazine known as the Silver Chert. This facies consists of total silification of limestone, silty limestone and sandstone. Brecciated textures in the Silver Chert appear to be

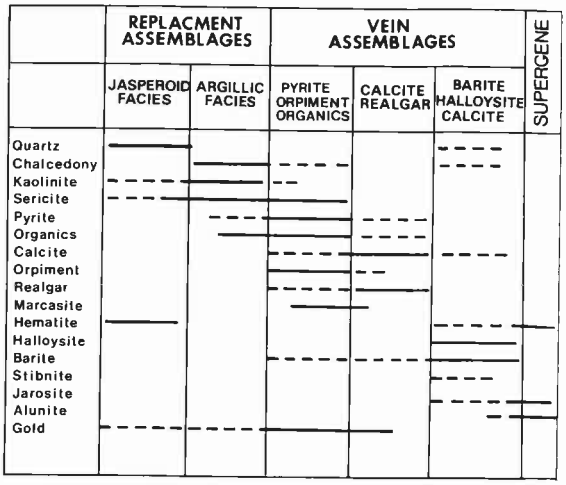

Fig. 2. Paragenetic sequence of hydrothermal alteration at Mercur.

a relic of karstification of the original limestone. Only minor amounts of jasperoid-facies rock are found outside of the Magazine Sandstone and Silver Chert.

Argillic-facies alteration consists of decarbonation of limestone and alteration of pre-existing phyllosilicate minerals. Argillic-facies alteration is present throughout the upper Topliff Member, but it is most common in silty limestone lithologies of the Mercur Beds, Upper Beds and lower portion of the Barren Beds. Argillic alteration was accomplished under early oxidized (no organic carbon, Fe present as hematitic material) and somewhat later reduced (hydrothermal organic material plus pyrite) hypogene conditions. Sericite and kaolinite are the only phyllosilicates in argillic- or jasperoid-facies rocks.

Three vein assemblages are recognized at Mercur. All are later than replacement assemblages (Fig. 2). The pyrite–orpiment–organics ± marcasite assemblage is found in the Mercur Beds and more rarely in the Barren Beds. Calcite, realgar and barite are minor associates of this assemblage. The pyrite–orpiment–organics ± marcasite assemblage often occurs as irregular masses in close spatial association with argillic-facies rocks.

The second vein mineral assemblage consists of sharply defined veins of calcite and realgar. The calcite–realgar veins rarely contain any other minerals. Calcite–realgar veins are found throughout the upper Topliff Member except where oxidized hydrothermal alteration is present.

The final hypogene vein assemblage consists of barite, halloysite, and minor calcite. The barite–halloysite–calcite veins are common in open spaces of the Silver Chert, although minor amounts are found throughout the upper Topliff section.

3. Analytical methods

3.1. Whole-rock analyses

Major- and minor-element determinations were made of selected samples of unaltered and altered lithologies at Mercur (Table I). Major elements were determined by standard X-ray fluorescence (XRF) spectrometry procedures. Minor elements were determined by a variety of analytical techniques (Table I). Mineral modes were calculated in the following manner for each sample. Weight percentages were converted to mole percentages. All K_2O was partitioned into illite or sericite and sufficient SiO_2, Al_2O_3, MgO, FeO and H_2O subtracted to form the appropriate illite or sericite stoichiometry (Table II). Remaining Al_2O_3 was combined with an appropriate amount of SiO_2 to form kaolinite. The remaining SiO_2 was calculated as quartz. MgO not partitioned into illite or sericite was combined with appropriate amounts of CaO and CO_2 to form dolomite. All remaining CaO and CO_2 was combined to form calcite. In all unoxidized rocks, the remaining Fe was combined with sulfur to form pyrite. In oxidized rock, all Fe was assumed to be Fe_2O_3. Modal partitioning of whole-rock analyses of the Silver Chert and Magazine Sandstone was done in a similar manner to that of other oxidized rocks except that K_2O was initially partitioned into jarosite, if that mineral was found by XRD. Mole percentages were then recomputed and presented in Table I as weight percentages.

3.2. Microprobe

Chemical compositions of 9 illite grains from an unaltered Upper Beds sample and 22 sericite grains from 4 altered samples were made with an ARL® microprobe equipped with EMX® wavelength-dispersive system (WDS) and TN Tracor Northern® energy-dispersive system (EDS). Hollister et al. (1984) have shown that EDS analysis is sufficiently accurate for elements of relatively high concentration (>1–5 wt.%). For the illites and sericites in this study, Na, Fe and Mg were analyzed by the relatively accurate WDS. Elements which had high concentrations (Si, Al, K) or which were not crucial for thermodynamic characterization (Ti, Mn, Ca) were analyzed by EDS. The microprobe was operated at 15-kV, 0.02-μA sample current. In general, six 10-s spots for WDS and one 50-s EDS accumulation were made on each grain. The sample was moved continuously to prevent vaporization of alkalis. A Tracor Northern® EDS visual display was used to detect interference from adjacent grains. All analyses were corrected for matrix effects using the procedures of Albee and Ray (1970).

Natural illites and sericites consist of varying amounts of muscovite ($KAl_3Si_3O_{10}(OH)_2$), paragonite ($NaAl_3Si_3O_{10}(OH)_2$), celadonite ($(K,Na,)(Fe,Mg)AlSi_4O_{10}(OH)_2$) and pyrophyllite ($Al_2Si_4O_{10}(OH)_2$) (Weaver and Pollard, 1973). Activities of muscovite, paragonite and pyrophyllite were calculated from microprobe analyses using relationships of Aagaard and Helgeson (1983).

3.3. Fluid inclusions

Heating and freezing measurements of fluid inclusions in selected hydrothermal minerals in the Mercur gold deposit were made using a Chaixmeca® heating–freezing microscope stage.

TABLE I

Whole-rock chemical analyses of upper Topliff Member, Great Blue Limestone at Mercur (numbers in parentheses are one standard deviation)

	(1) Massive Limestone (n=4)	(2) Silty Limestone (n=4)	(3) Silver Chert (n=3)	(4) Silicified Magazine Sandstone (n=3)	(5) Argillic-facies limestone (oxidized) (n=3)	(6) Argillic-facies limestone (partially, unoxidized) (n=5)	(7) Massive limestones with vein mineral assemblages (n=3)
SiO_2	6.42 (1.11)	34.55 (3.36)	94.14 (3.86)	89.37 (2.25)	41.81 (2.14)	66.12 (13.89)	15.66 (6.32)
TiO_2	0.06 (0.03)	0.34 (0.06)	0.16 (0.04)	0.45 (0.06)	0.34 (0.16)	0.41 (0.21)	0.14 (0.05)
Al_2O_3	1.01 (0.82)	5.99 (1.21)	1.76 (0.59)	4.71 (0.99)	7.65 (3.36)	9.09 (2.39)	2.35 (0.94)
Fe_2O_3			1.50 (1.27)	0.97 (0.45)	4.81 (3.74)		
FeO	0.89 (0.52)	2.12 (0.11)				3.51 (2.91)	1.06 (0.31)
MnO	0.13 (0.09)	0.09 (0.04)	0.01 (0.00)	0.01 (0.01)	0.08 (0.02)	0.02 (0.01)	0.19 (0.10)
MgO*[1]	0.39 (0.14)	0.72 (0.27)	0.05 (0.01)	0.20 (0.10)			
CaO	50.65 (3.76)	29.37 (2.10)	0.01 (0.00)	0.41 (0.40)	22.23 (4.14)	4.79 (5.35)	43.23 (4.52)
K_2O	0.11 (0.14)	1.01 (0.35)	0.45 (0.42)	1.10 (0.25)	1.00 (0.97)	1.30 (0.61)	0.33 (0.33)
Na_2O*[1]	0.00 (0.00)	0.05 (0.01)					
P_2O_5	0.50 (0.14)	0.44 (0.03)	0.00 (0.00)	0.00 (0.00)	0.24 (0.09)	0.13 (0.06)	0.48 (0.04)
SO_3*[2]			1.43 (1.04)	1.21 (0.86)	0.07 (0.01)		
S^{2-} *[2]	0.36 (0.53)	1.55 (0.28)				3.61 (2.24)	1.32 (0.54)
H_2O*[3]	0.65 (0.63)	2.69 (0.64)			3.21 (1.39)		1.07 (0.19)
CO_2*[4]	39.06 (1.22)	20.71 (1.74)			17.60 (2.79)		34.63 (3.38)
C_{org}*[5]	0.18 (0.14)	0.79 (0.50)			0.02 (0.03)	1.28 (0.84)	0.37 (0.03)
LOI			1.91 (1.07)	1.84 (1.44)		10.85 (4.36)	
Less O=S	0.08	0.34				0.73 (0.65)	0.30 (0.12)
Total	100.33	100.76	101.42	100.27	99.06	98.83	100.53
Quartz	5.32 (1.76)	26.35 (2.81)	92.08 (4.63)	82.96 (3.25)	31.55 (4.87)	54.02 (15.27)	12.47 (5.00)
Illite*[6]	1.64 (2.14)	15.07 (5.19)					3.64 (3.69)
Sericite*[6]			0.71 (1.00)	9.18 (2.26)	11.12 (10.78)	14.48 (6.77)	
Kaolinite	0.61 (0.68)	2.14 (2.61)	3.66 (0.93)	4.68 (1.07)	10.26 (6.19)	11.19 (6.66)	3.04 (2.65)
Calcite	89.10 (4.38)	44.69 (3.31)			39.26 (7.09)	8.25 (9.24)	77.84 (7.55)
Dolomite	1.77 (0.62)	3.23 (1.26)					
Pyrite	0.76 (1.01)	2.70 (0.34)				5.78 (4.44)	2.46 (1.01)
Jarosite			3.98 (3.07)	2.61 (0.73)			
Hematite			0.57 (0.71)				

	Silver Chert plus Magazine Sandstone (n=7)	Partially oxidized plus reduced samples (n=6)
As*[8]	842 (1,158)	11,366 (18,821)
Sb*[8]	989 (1,332)	19 (24)
Hg*[8]	12 (14)	27 (30)*[7]
Tl*[8]	47 (54)	178 (73)*[7]
Ag*[9]	0.130 (0.217)	0.018 (0.041)
Au*[9]	0.049 (0.047)	0.082 (0.091)

*[1]AAS; *[2]LECO® analysis; *[3]total water by Penfield analysis (Hutchinson, 1974); *[4]acid titration; *[5]method of Gaudette et al. (1974); *[6]analyses from Table II (all other elements by XRF); *[7]three analyses; *[8]ppm; *[9]ounces/ton.

Nearly 200 individual inclusions representing the jasperoid facies and two of the three major hypogene vein assemblages were analyzed (Table III). Standard thin-sections were used to identify individual crystals which contained usable fluid inclusions. Doubly polished plates ranging in thickness from 100 μm to 1 mm were then prepared from these samples. Only those

TABLE II

Microprobe analyses of illite and sericite

		HS-*4-1928* illite ($n=9$)	R-*21-90* sericite ($n=9$)	M-*6/22-6* sericite ($n=5$)	ML-*9-198* sericite ($n=5$)	ML-*9-214* sericite ($n=3$)
Compositions:						
	SiO_2	49.12 (1.22)	46.34 (1.37)	47.28 (1.14)	47.83 (1.38)	47.87 (1.55)
	TiO_2	0.84 (0.46)	0.47 (0.18)	0.45 (0.20)	0.41 (0.20)	0.54 (0.33)
	Al_2O_3	36.18 (1.17)	33.27 (2.14)	32.68 (2.74)	31.58 (2.06)	30.68 (3.61)
	FeO	0.35 (0.05)	2.34 (1.38)	3.56 (1.24)	2.50 (1.58)	1.73 (1.34)
	MnO	0.21 (0.05)	0.27 (0.08)	0.00	0.00	0.00
	MgO	0.89 (0.14)	1.03 (0.65)	1.38 (0.58)	1.40 (0.67)	1.67 (1.02)
	CaO	0.26 (0.12)	0.41 (0.40)	0.21 (0.06)	0.14 (0.01)	0.32 (0.01)
	K_2O	5.95 (0.32)	9.06 (1.11)	8.07 (1.32)	9.03 (1.25)	8.51 (0.37)
	Na_2O	0.42 (0.16)	0.52 (0.14)	0.31 (0.16)	0.30 (0.14)	0.41 (0.34)
	H_2O	5.50	4.72	5.16	4.70	4.67
	Total	99.72	98.43	99.10	97.89	96.40
Ions:						
	Si	3.18	3.12	3.16	3.22	3.26
	Ti	0.04	0.02	0.02	0.02	0.03
	Al^{IV}	0.82	0.88	0.84	0.78	0.74
	Al^{VI}	1.94	1.76	1.73	1.73	1.72
	Fe^{3+}	0.02	0.12	0.18	0.13	0.09
	Mn	0.01	0.02			
	Mg	0.09	0.10	0.14	0.14	0.17
	K	0.49	0.78	0.69	0.78	0.74
	Na	0.05	0.07	0.04	0.04	0.05
	Ca	0.02	0.03	0.02	0.01	0.02
Activities:						
	Mus	0.45	0.60	0.51	0.56	0.52
	Par	0.05	0.05	0.03	0.03	0.04
	Pyr	0.16	0.03	0.07	0.05	0.06

HS-*4-1928* = silty limestone from unaltered Upper Beds, DDH-HS-*4*.

R-*21-90* = totally decarbonated organic-rich siltstone, argillic facies, median limestone; Magazine Sandstone, DDH-R-*21*, Marion Hill.

ML-*9-198* = totally decarbonated organic-rich siltstone, argillic facies, with orpiment–pyrite–calcite–barite vein material; Mercur Beds, DDH-ML-*9* Mercur Hill.

M-*9/22-6* = decarbonated silicified organic-rich siltstone jasperoid and/or argillic facies, surface sample; Mercur Beds, Marion Hill.

ML-*9-214* = partially decarbonated organic-rich silty limestone, argillic-facies alteration with pyrite–orpiment–realgar vein material; Mercur Beds, DDH-ML-*9*, Mercur Hill.

Mus = muscovite; Par = paragonite; Pyr = pyrophyllite.

inclusions with characteristics which indicated a primary origin were analyzed (Roedder, 1979). Reproducibility of the heating measurements was ±3.0°C and ±0.4°C for the freezing point depressions. Calibration was made with standard organic materials of known melting points (MacDonald and Spooner, 1981) and NaCl–H_2O solutions of known salinity. Crushing stage measurements were made of selected samples to determine whether anoma-

TABLE III

Summary of fluid-inclusion data

Sample	Topliff interval	Mineral association	Filling temperature (°C)				Salinity (eq. wt.% NaCl)		
			No.	range	mean	S.D.	No.	range	mean
Quartz in jasperoid facies:									
GV-*25-212*	Upper Beds	quartz vein	3	252–258	256	3			
GV-*25-403*	Silver Chert	quartz in vug	10	208–290	237	27			
H-*17-237*	Magazine Sandstone	quartz vein	8	203–247	222	15	5	4.4–7.4	6.6
M-*9/22-5*b	Silver Chert	quartz in vug	5	230–303	265	32	2	6.4–6.7	6.9
Calcite associated with argillic-facies, pyrite-orpiment-organics-marcasite veins, and/or calcite-realgar veins:									
GV-*25-217*	Upper Beds	calcite–realgar vein in argillic-facies rocks	2	188–197	192	6			
GV-*25-242*	Mercur Beds	calcite vein with organics	7	175–196	187	8			
MH-*9-128*	Upper Beds	calcite–realgar vein	21	125–230	165	24			
MH-*9-130*	Upper Beds	calcite vein in argillic facies	2	138–167	153	21	5	5.8–8.9	7.2
MH-*9-156*	Mercur Beds	calcite–realgar vein	14	139–199	175	17			
MH-*9-292*	limestone in Magazine Sandstone	calcite vein in argillic-facies rock	2	174–178	176	3			
ML-*9-158*	Upper Beds	calcite–realgar vein	26	128–199	172	23	8	3.3–6.4	5.0
Barite-halloysite-calcite veins:									
M-*9/22*a	Silver Chert	barite in vug	20	272–253	308	21			
P-*27-118*	Silver Chert	barite in vug	24	145–278	218	27	14	5.5–7.9	7.0
P-*27-130*	Silver Chert	barite vein	10	152–321	268	51			
P-*27-149*	Silver Chert	barite in vug	13	161–315	235	51			
P-*27-156*	Silver Chert	barite in vug	17	155–231	186	22	12	2.1–4.8	3.8

S.D. = standard deviation (1σ).

lous internal pressures were present in the fluid inclusions.

Fluid-inclusion leach analyses were performed on cleaned crushed samples of hydrothermal calcite. All other minerals were deemed unsuitable for leach analysis due to fine grain size and/or contaminating mineral phases. 4–10 g of vein calcite were hand-picked, cleaned in dilute acid, and crushed in a mortar and pestle. The crushed sample was leached with doubly-distilled water and the leachate analyzed by inductively coupled plasma spectrometry (ICP)

TABLE IV

Summary of m_{Na+}/m_{K+} ratios of fluid-inclusion leach analyses

Sample	m_{Na+}/m_{K+}	Mean homogenization temperature (°C)	Comments
GV-*25-242*a	2.8	187	calcite vein with abundant organics
GV-*25-242*b	3.2	187	calcite vein with abundant organics
MH-*9-128*a	3.0	165	calcite-realgar vein
MH-*9-128*b	6.7	165	calcite-realgar vein
MH-*9-292*	9.2	176	calcite vein crosscutting argillic-facies rocks
ML-*9-158*	3.7	172	calcite-realgar vein
R-*21-94*a	3.1	-	calcite-realgar vein in organic-rich argillic-facies rocks
R-*21-94*b	1.6	-	calcite-realgar vein in organic-rich argillic-facies rocks

for K, Na and Ca. The amount of Ca in the leachate was approximately the same as (Na+K), indicating dissolution of the host mineral was minimal. K/Na ratios are reported in Table IV.

4. Chemical composition of unaltered rocks

Several generalizations can be drawn from the bulk chemistry of unaltered rocks (Table I). Massive limestones are essentially pure carbonates with <10% total silica, 0–2% alumina and trace amounts of pyrite. Relative amounts of kaolinite and illite are difficult to characterize, given the small number of samples (4) and the small percentages of clay minerals. Four thinly bedded, silty limestones have 30–40% silica and 5–10% alumina. Modal partitioning of elements shows that illite/kaolinite ratios are near unity. The amount of pyrite is between 1% and 3%. The unaltered Topliff samples have organic carbon contents within the 0.2–1.0% range reported for unaltered Great Blue rocks outside of the Mercur district (W. Tafuri, pers. commun., 1982).

Microprobe analyses of illite from unaltered rocks shows less K_2O, more SiO_2, MgO and H_2O than muscovite, but less MgO and Fe_2O_3 than hydrothermal sericite (Table II). Interlayer site occupancy is typically <0.6, possibly due to interstratification with smectite layers.

5. Chemical composition of altered rocks

5.1. Bulk chemistry

Modes calculated from whole-rock analyses show that quartz constitutes 85–97% of jasperoid-facies rocks (Table I, columns *3* and *4*). Kaolinite appears to be the dominant phyllosilicate in the Silver Chert, whereas sericite is more common in the Magazine Sandstone.

Whole-rock chemical analyses of argillic-facies rocks are consistent with simple decarbonation of silty limestones. Deposition of silica in the argillic facies was minor. Silica values range up to 75–80% in totally decarbonated limestones (Table II, columns *5* and *6*). This twofold increase in silica contents of unaltered silty limestones is the result of dissolution of original carbonate (50–60% of the original total).

Mineral modes of argillic-facies rocks and unaltered silty and shaley limestones show a progression in terms of oxidation and carbonate content (Fig. 3). Four unaltered samples have calcite contents of 40–50%. Argillically altered limestones have variable amounts of calcite (2–50%). Of particular note is the progression from oxidized high-calcite samples

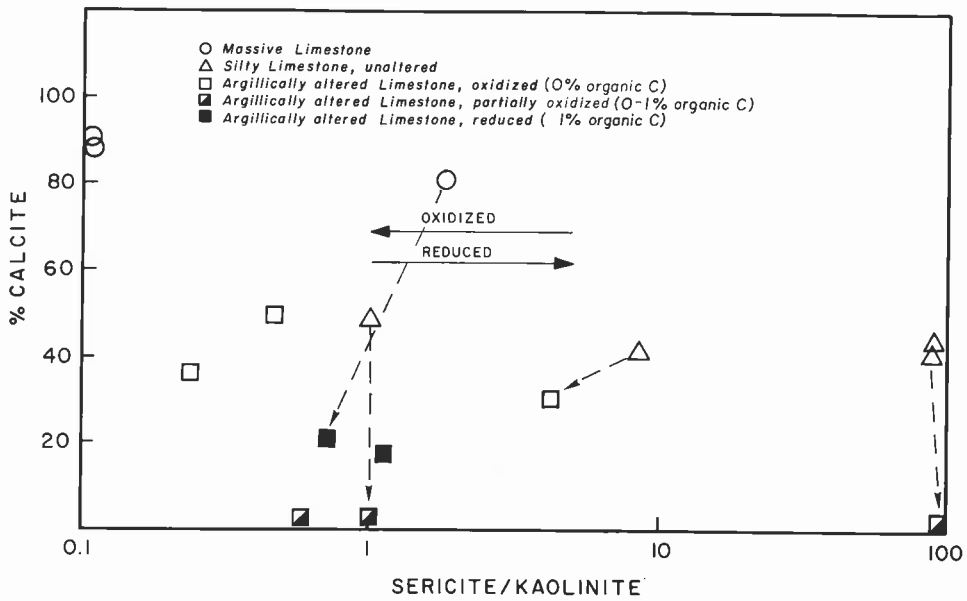

Fig. 3. Percent calcite vs. (sericite/kaolinite) plot for unaltered and argillically altered rocks at Mercur. Sericite/kaolinite ratios of 0.1 and 100 correspond to zero and infinity, respectively. *Tie-lines* show unaltered/altered samples which are stratigraphically equivalent.

to reduced totally-decarbonated samples. The geochemical significance of this observation is discussed in Section 7.4.2.

Sericite/kaolinite ratios are variable for all samples (Fig. 3). Where unaltered and altered limestone were analyzed from the same sample or an equivalent stratigraphic horizon, the altered rocks retain a sericite/kaolinite ratio which was essentially unchanged, despite the chemistry of hydrothermal sericite being significantly different than sedimentary illite (Table II).

Three whole-rock analyses were made of massive limestones with calcite–realgar veins (Table I, column 7). Chemical composition of the rock hosting the calcite–realgar veins is similar to that of massive unaltered limestones, indicating that formation of the veins did not significantly alter the enclosing rock.

5.2. Sericite analyses

Sericites have slightly lower amounts of silica and alumina than the analyzed illites, and the total interlayer site occupancy is greater in the sericites than in the illites (Table II). Octahedral Fe and Mg are somewhat higher in sericites than in illites, an observation which may account for the characteristic green color of sericite in thin-section. Composition of the sericites is similar to those reported in modern geothermal systems and other ore deposits (McDowell and Elders, 1980; Parry et al., 1984).

5.3. Precious-metal and trace-element spatial distribution

The paragenesis of Au has not been unequivocally documented in any Carlin-type Au deposit, including Mercur. At Mercur, the extremely fine-grained nature of the Au prevented its identification in polished section. Ore-grade Au is associated with specific alteration types and stratigraphic intervals at Mercur, however. This association allows some constraints to be place on the timing and mechanisms of Au mineralization.

The bulk of Au mineralization occurs in the Mercur Beds in conjunction with argillic-facies alteration and/or the pyrite–orpiment– organ-

ics ± marcasite vein assemblage. Samples from the Mercur Beds with high Au values frequently have a strong As–Tl–Hg geochemical signature, even if no As minerals are visible (Mercur geologic staff, pers. commun., 1982). Cinnabar has been reported at Mercur (Gilluly, 1932) but was not observed in this study, and no Tl minerals were identified at Mercur.

The Silver Chert and silicified Magazine Sandstone are hosts for significant amounts of Au mineralization. Silica encapsulation of the gold has not been noted (W. Tafuri, pers. commun., 1982), suggesting that Au deposition followed silica deposition. Historical records indicate that the Silver Chert–Magazine Sandstone interval was host for virtually all of the Ag production in the Mercur district (Spurr, 1895; Butler et al., 1920). Specific Ag minerals were not observed in this study, although geochemical assays occasionally show anomalous Ag concentrations in the Silver Chert. The Silver Chert also has an As–Sb–Tl–Hg trace-element signature, but stibnite is the only mineralogical manifestation of these elements.

The Upper and Barren Beds show locally significant amounts of Au mineralization. Alteration and trace-element signatures in such cases resemble those in the Mercur Beds.

6. Fluid inclusions

Fluid inclusions suitable for heating and freezing measurements were found in euhedral quartz overgrowths on earlier fine-grained quartz in the Silver Chert. Care was taken to distinguish this early quartz from the much rarer quartz deposited in the barite–halloysite veins. One sample of fluid inclusion-bearing quartz was identified from the Upper Beds (GV-*25-212*, Table III). In this sample, quartz grains are crosscut by realgar, thus establishing the quartz as the earlier formed mineral.

Fluid inclusions in quartz are sparsely and irregularly distributed throughout individual quartz crystals. Diameters are generally <15 μm. All inclusions are two-phase, liquid dominant with no daughter minerals.

Fluid inclusions in hydrothermal calcite were measured where calcite veins crosscut earlier hydrothermal minerals or contained realgar. The inclusions are abundant and evenly distributed, but generally quite small (2–10 μm) although 20–30-μm inclusions are not uncommon. All inclusions are two-phase, liquid dominant.

Fluid inclusions are abundant in virtually all of the barite found at Mercur. Barite fluid inclusions exhibit a wide variety of shapes and sizes (up to 25 μm in diameter) and many appear empty or have a high vapor/liquid ratio. This feature can be explained as entrapment of varying proportions of liquid and vapor by a boiling fluid or as leakage through prominent cleavage planes in the barite due to internal pressures produced by carbon dioxide. Homogenization of the vapor-rich inclusions was not achieved, even at very high temperatures. This seems to indicate that the vapor-rich inclusions were the result of leakage rather than boiling. Heating measurements of liquid-dominant barite fluid inclusions were as reproducible as those in quartz and calcite and suggest that little leakage has occurred during measurement. The standard deviations for barite-filling temperatures are somewhat higher than those of quartz and calcite (Table III).

Recent research (Bodnar and Bethke, 1984) has demonstrated that stretching of fluid inclusions can occur when soft host minerals are overheated. The effect is most pronounced in relatively large fluid inclusions. Fluid inclusions with a volume of 10^5 μm^3 in fluorite and sphalerite are stretched by overheating of only 30°C (Bodnar and Bethke, 1984). For the Mercur samples analyzed in this study, the average volumes of the calcite and barite fluid inclusions were $10^{2.5}$ and 10^3 μm^3, respectively. Errors due to overheating may be less pronounced in these relatively small inclusions.

Assuming that fluids which deposited barite were hotter than those which deposited hydro-

thermal calcite, overheating and stretching of the calcite fluid inclusions is a possibility. If so, the calcite depositional temperatures were actually somewhat lower than the homogenization temperatures reported in Table III.

Freezing measurements were performed on quartz, calcite and barite although the small size of most fluid inclusions often precluded determination of the final melting point of the ice. Salinities (expressed as eq. wt.% NaCl in Table III) were computed using the equations of Potter et al. (1978). No CO_2 clathrates were observed nor was liquid CO_2 seen during any cooling runs. Crushing stage analyses produced bubbles in the surrounding oil, however. These bubbles are the result of gases with positive internal pressures in the fluid inclusions. The most common gas to produce this sort of pressure is CO_2 (Bodnar et al., 1985).

Observations of first melting during fluid inclusion freezing runs and fluid inclusion leach analyses allow broad generalizations of fluid composition to be made. Although first melting was difficult to see, it appeared to occur at temperatures no lower than $-25°C$, with temperatures of $\sim -20°C$ more typical. Divalent cations (Ca^{2+} and Mg^{2+}) depress the eutectic (first melting) of aqueous brines significantly (up to $-50°C$). The observations of the eutectic in Mercur fluid inclusions indicate that the mole fraction of univalent cations (Na^+ and K^+) is greater than divalent cations (Crawford, 1981). Fluid-inclusion leach analyses of hydrothermal calcite show Na/K molar ratios which vary from 1.6 to 9.7 although most values are between 3 and 5.

Fluid inclusions in jasperoid-facies quartz show that temperatures of the initial Mercur fluids ranged from 220° to 270°C. The fluids apparently had cooled by the time of vein deposition, as shown by filling temperatures of hydrothermal calcite (150–190°C). During the final barite–halloysite stage, the fluids were heated to the 180–300°C temperature range. Considering the tendency of barite fluid inclusions to stretch, the lower portion of this temperature range is probably more realistic. Throughout the paragenesis at Mercur, the salinity of the fluids remained relatively constant at 5–8 eq. wt.% NaCl (Table III). In the few fluid inclusions where both heating and freezing measurements were accomplished a weak positive correlation is observed between temperature and salinity. Such correlations are considered indicative of high-salinity high-temperature fluids mixing with cool dilute groundwater. The data are too few to confirm this at Mercur, although geochemical considerations discussed in Section 8 also suggest fluid mixing.

Fluid-inclusion studies at the Carlin Au deposit (Radtke et al., 1980) have shown a thermal history which has some similarities to the Mercur deposits. In both deposits, ore stage deposition at temperatures of 160–200°C is followed by a sulfate stage in which depositional temperatures were higher (>200°C). Unlike Carlin, Mercur shows early jasperoid deposition at relatively high temperature (up to 240°C). At Carlin, jasperoid deposition is interpreted as part of a late-stage acid–sulfate event associated with boiling.

Fluid inclusions at Mercur do not provide positive confirmation of boiling hydrothermal fluids. If total pressure is equal to:

$$p_f = p_{H_2O} + p_{CO_2}$$

a free vapor phase can form and coexisting vapor and liquid can be trapped in fluid inclusions; lack of recognition of vapor-rich inclusions does not prove nonboiling conditions (Hedenquist and Henley, 1985). Mineral assemblages present in boiling zones of geothermal systems that also appear in epithermal vein systems suggest that boiling is common in epithermal systems. The diagnostic minerals include calcite (present as discrete veins at Mercur) and hydrothermal K-feldspar (not observed at Mercur).

A plot of calcite fluid-inclusion filling temperatures against present day elevation above sea level is given in Fig. 4. A linear least-squares

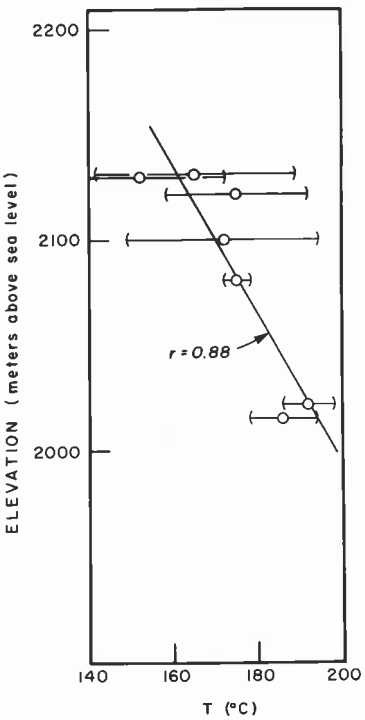

Fig. 4. Calcite fluid-inclusion filling temperatures plotted against present-day elevation at Mercur.

fit through the mean value of each sample indicates a fluid temperature gradient of 30°C/100 m. Gradients this high are indicative of vertical fluid flow in a shallow subsurface environment (Rybach and Muffler, 1981; Vikre, 1985). This gradient also correlates with the boiling curve of H_2O under hydrostatic conditions at depths of 100–400 m (Haas, 1971).

7. Geochemical model

Fluid-inclusion observations and mineral assemblages present in the Mercur deposit are used to establish limits to intensive geochemical parameters of the alteration assemblages. Mineral assemblages at Mercur, fluid-inclusion characteristics, available thermodynamic and experimental data, together with chemical characteristics of modern geothermal systems permit estimation of limiting values of pH, fugacities of CO_2, O_2 and H_2S, activities of Na, K, Ca, H_2S and SO_4, and postulation of principal Au precipitating mechanisms. Reactions relevant to these geochemical parameters are summarized in Table V.

The Upper Beds, Mercur Beds and Barren Beds contain oxidized and reduced argillic-facies alteration and all vein minerals. Although three separate vein assemblages are described, there is temporal and spatial overlap in deposition of all vein minerals and argillic alteration (Fig. 2). Calcite and realgar form distinct veins with no other minerals, but small amounts of calcite and realgar also occur in the pyrite–orpiment–organics ± marcasite assemblage. Minor amounts of barite are also found with this assemblage. This suggests that deposition of realgar, orpiment, pyrite, marcasite, calcite and barite was approximately contemporaneous. The geochemical model discussed in this section is based on stabilities of these minerals as well as fluid-inclusion data.

In the silicified oxidized Silver Chert and Magazine Sandstone, only very general geochemical constraints can be established, due to the restricted number of alteration minerals.

7.1. Temperature and salinity

A typical temperature for jasperoid replacement of limestone is 240°C, the mean T_h for fluid inclusions in quartz (Table III). Jasperoid-facies salinity used in subsequent calculations is 6.4 eq. wt.% NaCl, which gives an ionic strength of 1.0 and $m_{Cl^-} = 1.0$ at 240°C using the computer program SOLVEQ (Reed, 1982).

The fluid-inclusion filling temperatures of hydrothermal calcite range between 153° and 192°C. For the argillic facies–vein assemblage model, a temperature of 180°C is chosen in order to more closely approximate relevant experimental mineral solubility studies which usually have minimum temperatures of 175–200°C. Salinity is chosen to be the median of fluid-inclusion freezing measurements, or ~5.5 eq. wt.% NaCl (Table III).

TABLE V

Summary of thermodynamic data

Reaction	log K		Reference*[1]
	180 °C boiling curve	240 °C boiling curve	
(*1*) Muscovite-kaolinite $2KAl_3Si_3O_{10}(OH)_2+2H^++3H_2O\rightleftharpoons3Al_2Si_2O_5(OH)_4+2K^+$	4.70	4.14	(*a*)
(*2*) Paragonite-kaolinite $2NaAl_3Si_3O_{10}(OH)_2+2H^++3H_2O\rightleftharpoons3Al_2Si_2O_5(OH)_4+2Na^+$	8.94	7.70	(*a*)
(*3*) K-feldspar-muscovite $3KAlSi_3O_8+2H^+\rightleftharpoons KAl_3Si_3O_{10}(OH)_2+6SiO_{2\,(aq)}+2K^+$	−6.76	−5.24	(*a*)
(*4*) Quartz $SiO_2\rightleftharpoons SiO_{2\,(aq)}$	−2.51	−2.21	(*a*)
(*5*) Chalcedony $SiO_2\rightleftharpoons SiO_{2\,(aq)}$	−2.33	−2.06	(*a*)
(*6*) Calcite $CaCO_3+2H^+\rightleftharpoons Ca^{2+}+CO_{2\,(g)}+H_2O$	8.89	8.76	(*a*)
(*7*) Witherite $BaCO_3+2H^+\rightleftharpoons Ba^{2+}+CO_{2\,(g)}+H_2O$	4.55	4.80	(*a*)
(*8*) Anhydrite $CaSO_4\rightleftharpoons Ca^{2+}+SO_4^{2-}$	−6.67	−7.97	(*a*)
(*9*) Barite $BaSO_4\rightleftharpoons Ba^{2+}+SO_4^{2-}$	−9.83	−10.58	(*a*)
(*10*) Hematite-pyrite $Fe_2O_3+4H_2S_{(g)}+\frac{1}{2}O_{2\,(g)}\rightleftharpoons FeS_2+4H_2O$	34.22	26.84	(*a*)
(*11*) Magnetite-pyrite $Fe_3O_4+6H_2S_{(g)}+O_{2\,(g)}\rightleftharpoons3FeS_2+6H_2O$	62.05	49.33	(*a*)
(*12*) Magnetite-hematite $2Fe_3O_4+\frac{1}{2}O_{2\,(g)}\rightleftharpoons3Fe_2O_3$	21.44	18.13	(*a*)
(*13*) Realgar-orpiment $4AsS+S_{2\,(g)}\rightleftharpoons2As_2S_3$	12.07		(*b*)
(*15*) Sulfate-hydrogen sulfide $SO_4^{2-}+2H^+\rightleftharpoons H_2S_{(g)}+2O_{2\,(g)}$	−69.88	−56.88	(*a*)
(*16*) S_2-hydrogen sulfide $S_{2\,(g)}+2H_2O\rightleftharpoons2H_2S_{(g)}+O_{2\,(g)}$	−33.64	−28.43	(*a*)
(*17*) Gold $Au_{(s)}+2Cl^-+\frac{1}{4}O_2+H^+\rightleftharpoons\frac{1}{2}H_2O+AuCl_2^-$	2.02 7.23*[2] 8.27		(*a*) (*c*) (*d*)
(*18*) Gold $Au_{(s)}+2H_2S_{(aq)}+\frac{1}{4}O_2\rightleftharpoons\frac{1}{2}H_2O+H^++Au(HS)_2^-$	6.64		(*e*)

*[1]*References*: *a*=Helgeson (1969); Helgeson et al. (1978); *b*=Craig and Barton (1973); *c*=Drummond (1981); *d*=Wood (1985); *e*=Seward (1973).

*[2]Used in Fig. 5.

7.2. p_{CO_2}

Fluid-inclusion fluids in the Mercur samples are expected to contain carbon dioxide. The presence of mineralized and altered rocks in carbonaceous calcareous sedimentary rocks, and the chemical and petrographic evidence for dissolution of carbonates by the solutions requires carbon dioxide at some concentration level in the fluids. Careful observation of the fluid inclusions during freezing runs failed to show evidence of nucleation of a clathrate compound. However, the vapor bubble does expand when fluid inclusions are opened. Repeated freezing of fluid inclusions in calcite to $\sim -80°C$ and warming to 20°C to search for these effects opened inclusions along cleavage planes and permitted leakage which was always accompanied by expansion of the vapor bubble. Crushing stage measurements of jasperoid-facies quartz, vein calcite and vein barite plates containing fluid inclusions produced numerous small bubbles which rapidly coalesced into larger bubbles in the surrounding oil. These represent the contents of fluid inclusions that have expanded and indicates an internal pressure greater than atmospheric. This pressure is most commonly the result of carbon dioxide in the fluid inclusion (Bodnar et al., 1985).

Maximum p_{CO_2} possible in Mercur hydrothermal fluids is established from other fluid-inclusion characteristics. Clathrate was not observed to be present in the quartz fluid inclusions above 0°C. The low-temperature phase relations in the H_2O–CO_2–NaCl system (Collins, 1979; Hedenquist and Henley, 1985) indicate p_{CO_2} at 0°C of <20 bar within the fluid inclusions. Application of Henry's law ($K_h = p_{CO_2}/m_{CO_2}$) from Drummond (1981) gives $m_{CO_2} = 0.83$. K_h at 240°C in a 6.4 wt.% NaCl solution is 138 so maximum $p_{CO_2} = 115$ bar. Clathrate was also not observed at 0°C in calcite fluid inclusions. K_h in a 5.5 wt.% NaCl solution at 180°C is 141 (Drummond, 1981) so p_{CO_2} is <113 bar.

Dissolved CO_2 of these magnitudes in fluid inclusions can produce errors in salinity estimates of 0.6–3.2 wt.% NaCl (Hedenquist and Henley, 1985). Implications of this are discussed in Section 7.3.2.

7.3. Na, K, Ca and H activities

7.3.1. Jasperoid facies. Calcite dissolution is characteristic of jasperoid-facies alteration. pH of the jasperoid-forming fluids can be determined from the reaction:

$$\underset{\text{(calcite)}}{CaCO_3} + 2H^+ \rightarrow Ca^{2+} + CO_{2(g)} + H_2O \qquad (1)$$

If maximum p_{CO_2} and $a_{Ca^{2+}}$ are known, a minimum pH can be established. Maximum p_{CO_2} was determined above to be 115 bar. Maximum $a_{Ca^{2+}}$ is provided by the observations of approximate eutectic temperatures in quartz fluid inclusions. Since first melting of ice was not observed below $-20°$ to $-25°$C:

$$m_{Na^+} + m_{K^+} > m_{Ca^{2+}} + m_{Mg^{2+}}$$

The concentration of Mg^{2+} in hydrothermal solutions is usually small (Fournier and Truesdell, 1973); therefore, a charge balance can be assumed as:

$$m_{Na^+} + m_{K^+} + 2m_{Ca^{2+}} = m_{Cl^-} \sim 1 \text{ molal} \qquad (2)$$

This relationship implies $m_{Ca^{2+}} < 0.33$. $a_{Ca^{2+}}$ is then computed as <0.05 using the high-temperature activity coefficients of Wood et al. (1985). Substituting these values into an expression for the equilibrium constant for reaction (1) gives a minimum pH of 3.6.

7.3.2. Argillic facies–vein assemblages. The transition from calcite-undersaturated conditions (argillic-facies alteration) to calcite-saturated conditions (vein assemblages) is observed in close spatial association at Mercur. Aluminosilicate mineral equilibria in conjunc-

tion with calcite equilibria can therefore place upper and lower bounds on cation activities of argillic facies–vein assemblages.

Coexisting kaolinite and hydrothermal sericite is found in virtually all argillic-facies rocks (Table I; Fig. 3). Since sericite is the only K- and Na-bearing mineral phase at Mercur, it is logical to assume that it was controlling the a_{K^+}/a_{H^+} and a_{Na^+}/a_{H^+} ratio of the fluid. Equilibrium constants for the kaolinite–muscovite and kaolinite–paragonite reactions (Table V) in conjunction with the activities of muscovite and paragonite in analyzed sericite (Table II) allow these ratios to be determined:

$$3Al_2Si_2O_5(OH)_4 + 2K^+ \rightleftharpoons$$

(kaolinite)

$$2KAl_3Si_3O_{10}(OH)_2 + 2H^+ + 3H_2O \qquad (3)$$

(muscovite in sericite)

with

$$\log K_{eq} = -4.18$$

$$3Al_2Si_2O_5(OH)_4 + 2Na^+ \rightleftharpoons$$

(kaolinite)

$$2NaAl_3Si_3O_{10}(OH)_2 + 2H^+ + 3H_2O \qquad (4)$$

(paragonite in sericite)

with

$$\log K_{eq} = -6.14$$

Combining eq. 3 with eq. 4 gives $a_{Na^+}/a_{K^+} = m_{Na^+}/m_{K^+} = 9.1$. Fluid-inclusion leach analyses suggest m_{Na^+}/m_{K^+} of 3–5 (Table IV). Given the analytic uncertainty of the microprobe and fluid-inclusion techniques, the agreement between these two estimates is very reasonable.

$a_{Ca^{2+}}/a_{H^+}^2$ and p_{CO_2} can be established using the calcite solution–dissolution equilibria (eq. 1). $m_{Ca^{2+}} < 0.33$ molal and $p_{CO_2} < 113$ bar have been established from fluid-inclusion observations discussed above. Inserting these values into eq. 1 gives a minimum pH of 4.0.

A minimum pH of 4.0 establishes a maximum m_{K^+} of 0.03 molal (eq. 3) and maximum m_{Na^+} of 0.09–0.27 molal. These estimates are in disagreement with fluid-inclusion eutectic measurement which imply that:

$$m_{Na^+} + m_{K^+} > m_{Ca^{2+}}$$

Progressively lower p_{CO_2}-values (eq. 1) imply progressively higher pH and hence lower cation activities (eqs. 3 and 4).

One resolution to these inconsistencies may be found in the arguments of Hedenquist and Henley (1985). They show that modest amounts of CO_2 (0.2–1.0 molal) in hydrothermal fluids can result in overestimation of salinity by as much as 3.2 wt.% NaCl. Thus, if eq. 2 were modified to read $m_{Cl^-} = 0.5$ molal, more reasonable maximum cation estimations of $m_{Ca^{2+}} < 0.15$, $m_{K^+} = 0.04$–0.05, and $m_{Na^+} = 0.12$–0.45 could be made by the analysis given above. A maximum p_{CO_2} of 113 bar then gives a minimum pH of 3.7. With these assumptions, eqs. 1–3 are all satisfied.

Although the preceding discussion represents only estimations of pH, p_{CO_2}, and cation activities, the model does suggest some general conclusions. The spatial and temporal association of calcite solution–dissolution with the kaolinite–sericite mineral assemblage requires a relatively low-pH, high-p_{CO_2} fluid. The amount of CO_2 in epithermal environments is currently controversial (e.g., Hedenquist, 1986; Vikre, 1986). Some epithermal systems in volcanic rocks are known to have m_{CO_2} on the order of 0.5 molal (Ellis, 1979; Hedenquist and Henley, 1985). For hydrothermal fluids in thick carbonate sequences such as those which underlie Mercur the modestly high carbon dioxide pressure being hypothesized here ($m_{CO_2} = 0.8$) is not unreasonable.

7.4. f_{O_2} and f_{H_2O}

7.4.1. Jasperoid facies. In all examples of jasperoid-facies alteration at Mercur (Fig. 2), hematite is the dominant Fe-bearing phase. This appears to be universally true in the Silver Chert horizon where pyrite has not been observed. Although pyrite is a minor constituent of the massive limestones in Silver Chert equivalent rocks, the fact that hematite replaced pyrite during silicification establishes a minimum log f_{O_2} of ~ -34 to ~ -32, depending on the total sulfut and pH of the fluids [reaction (*10*), Table V].

7.4.2. Argillic facies-vein assemblages. Silty and shaley limestones which host argillic-facies alteration show a progressive evolution in terms of oxidation. As shown in Fig. 3, four unaltered silty limestone samples have calcite contents of 40–50% and highly variable illite to kaolinite ratios. Oxidized, argillically altered limestones have lower amounts of calcite (2–50%), and sericite/kaolinite ratios which are essentially the same as unaltered samples. A plausible interpretation is that early argillic-facies fluids were similar in composition to jasperoid-facies fluids, i.e. oxidizing and sufficiently acid to be in equilibrium with kaolinite and sericite. Whole-rock analyses of argillically altered silty limestones which are partially oxidized or reduced contain significantly less calcite (0–30%) and sericite/kaolinite ratios which are the same as unaltered rocks. This suggests that progressive decarbonation of the silty limestones was accomplished by fluids which were less oxidized. Reduction of the oxidizing fluids could have been accomplished by indigenous organic material in the limestones according to the reaction:

$$2CH_2O + 2H^+ + SO_4^{2-} \rightleftharpoons H_2S + 2H_2CO_3 \qquad (5)$$

where CH_2O is a generalized formula for sedimentary organic matter.

Log f_{S_2} of the vein assemblages can be fixed by realgar–orpiment coexistence [reaction (*13*), Table V)] at -12.07 (Craig and Barton, 1973). A lower limit of f_{O_2} can be established from the presence of calcite and the absence of anhydrite at Mercur [from reactions (*6*), (*8*), (*15*) and (*16*), Table V]:

$$\underset{\text{anhydrite}}{2CaSO_4} + 2CO_2 \rightarrow \underset{\text{calcite}}{2CaCO_3} + S_2 + 3O_2 \qquad (6)$$

with

$$\log K_{eq} = -137.3$$

Using f_{S_2} established by realgar–orpiment coexistence, log $f_{O_2} \sim -40.4$ at p_{CO_2} of 113 bar.

In a similar fashion, an upper limit is established by the occurrence of barite rather than witherite:

$$\underset{\text{barite}}{2BaSO_4} + 2CO_2 \rightarrow \underset{\text{witherite}}{2BaCO_3} + S_2 + 3O_2 \qquad (7)$$

with

$$\log K_{eq} = -134.9$$

Calculated values are near log $f_{O_2} = -39.6$ for the estimated p_{CO_2}. These f_{O_2}-values are approximately $\frac{1}{2}$ to 1 log unit smaller than the hematite–pyrite buffer (Fig. 5). The spatial association of these vein assemblages minerals with decarbonated limestones which show evolution from oxidized to reduced conditions suggests that f_{O_2} may have been somewhat variable.

Experimental work on the stability of marcasite provides additional evidence that the vein assemblages formed at f_{O_2}-values slightly lower than the hematite–pyrite buffer. Rising (1973) indicated that marcasite forms as a metastable product near the pyrrhotite–pyrite or pyrite–hematite boundaries. More recently, ElDahhar and Barnes (1979) and Murowchick and Barnes (1986) have indicated that marcasite forms in the presence of metastable intermediate-valence sulfur species according to reactions such as:

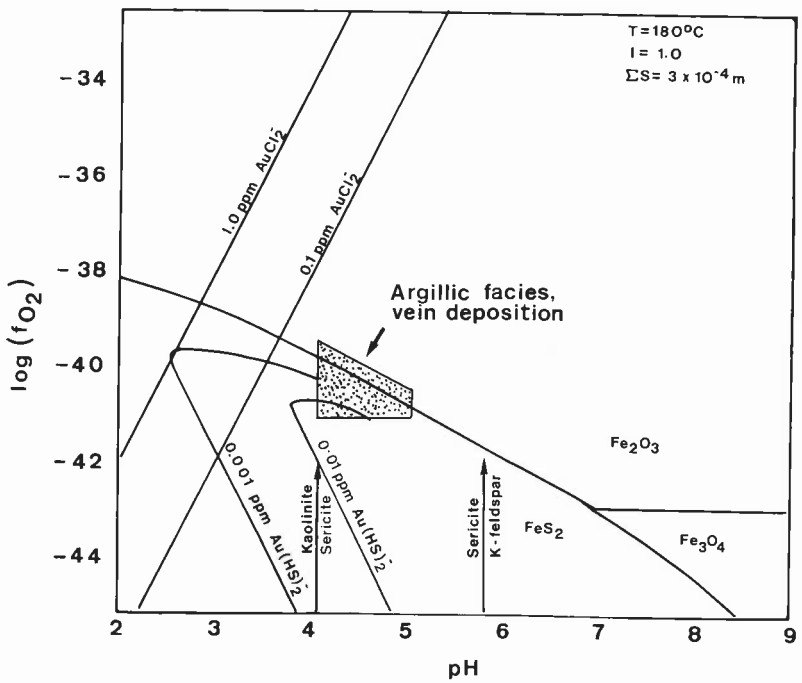

Fig. 5. pH vs. log f_{O_2} plot of argillic facies–vein assemblage fluids. $\Sigma S = 3 \cdot 10^{-4}$ molal estimated using log f_{O_2} from eq. 6 of the text and pH = 4.5. *Stippled area* represents ore-forming solutions at Mercur.

TABLE VI

Summary of chemical parameters of Mercur hydrothermal fluids

	Jasperoid facies	Argillic facies–vein assemblages
p_{CO_2} (bar)	<115	113
pH	>3.6	4.0–5.0
a_{K^+}		0.025
a_{Na^+}		0.07–0.22
$a_{Ca^{2+}}$		<0.03
log f_{O_2}	> −34 to −32	−40.4 to −39.6
log f_{S_2}		−12.07
log f_{H_2S}		−3.1 to −2.7
log m_{H_2S}		−4.7 to −4.3
log $m_{SO_4^{2-}}$		−4.5 to −1.3
Total S		$5 \cdot 10^{-5}$–$5 \cdot 10^{-2}$
Mineral assemblages	quartz, sericite, kaolinite, hematite	sericite, kaolinite, pyrite, orpiment, realgar, calcite, barite

$$4Fe^{2+} + 3S_2O_3^{2-} + 4H_2S \rightleftharpoons 4FeS_2 + 2SO_4^{2-} + 6H^+ + H_2O \quad (8)$$

marcasite

$$Fe^{2+} + H_2S_2 \rightleftharpoons FeS_2 + 2H^+ \quad (9)$$

marcasite

$S_2O_3^{2-}$ is not stable in hydrothermal solutions above 200°C (Barnes, 1979) and reaction (9) takes place below 160°C (Murowchick and Barnes, 1986). Marcasite forms abundantly only for conditions below pH 5 and below 240°C (Murowchick and Barnes, 1986). These temperature limits are consistent with our fluid-inclusion data from Mercur hydrothermal calcite (Table III) and for our estimated range of pH (Table VI).

Using the f_{O_2} constraints provided above allows a_{H_2S} of the argillic facies–vein assemblages

to be defined according to the reaction:

$$H_2S_{(g)} + O_2 \rightleftharpoons H_2O + S_2 \quad (10)$$

Calculated values of $\log f_{H_2S}$ are -3.1 to -2.7 using the estimated f_{S_2} and f_{O_2} conditions hypothesized above.

Total dissolved sulfur in Mercur hydrothermal fluids may be estimated. $H_2S_{(aq)}$ is calculated from Henry's law constant ($K_h = f_{H_2S}/m_{H_2S} = 46.2$ at 180°C) and $m_{NaCl} = 1.0$ (Drummond, 1981). Equilibrium constants for oxidation and dissociation reactions in Table V together with activity coefficients calculated with the aid of the computer program SOLVEQ (Reed, 1982) permit calculation of molalities of HS^-, SO_4^{2-} and HSO_4^-. Total dissolved sulfur molality is $\sim 3 \cdot 10^{-4}$ (assuming a median pH of 4.5 and $\log f_{O_2}$ from calcite–anhydrite, eq. 6).

8. Discussion of the ore-forming environment

The geological characteristics and geochemical parameters estimated above for formation of replacement and vein mineral assemblages provide important constraints on the chemical environment of Au ore precipitation, but only indirect evidence for the identity of the Au complex in solution is provided.

The earliest formed alteration at Mercur is replacement of massive and karst limestone below the Magazine Sandstone by massive jasperoid. Decarbonation of silty limestones in the Upper Beds, Mercur Beds and Barren Beds with deposition of minor quartz and chalcedony was contemporaneous with to slightly later than jasperoid formation.

Jasperoid formation in selected stratigraphic horizons (Silver Chert and Magazine Sandstone) implies that the hydrothermal fluids were silica saturated at these sites. This can be explained by cooling or by mixing of hydrothermal fluids with cold meteoric groundwater. Mixing of thermally-contrasting silica-undersaturated fluids is a logical mechanism for formation of silica-supersaturated fluids (Truesdell and Fournier, 1977) (Fig. 6). Relatively cold meteoric water might be expected in the porous Magazine Sandstone and underlying karst limestones. The Upper Beds, Mercur Beds and Barren Beds are much less porous and permeable than the Magazine Sandstone and underlying karst limestones, and they probably contained much less cold meteoric groundwater. Silica supersaturation would therefore be less likely, and hence these beds contain relatively little jasperoid.

The Silver Chert is completely oxidized. It is unlikely that this is the result of supergene alteration because there is a total lack of sulfides in even the most impermeable jasperoid. Evidence for hypogene oxidation being overprinted by unoxidized fluids during argillic-facies alteration is also compelling in thin section. A plausible explanation is that H_2S-bearing near-neutral pH fluids were oxidized by cool groundwater in the Silver Chert/Magazine Sandstone. The resulting acidic silica-supersaturated fluids dissolved limestone as they formed jasperoid. This evolved oxidized acidic fluid migrated into the Upper, Mercur

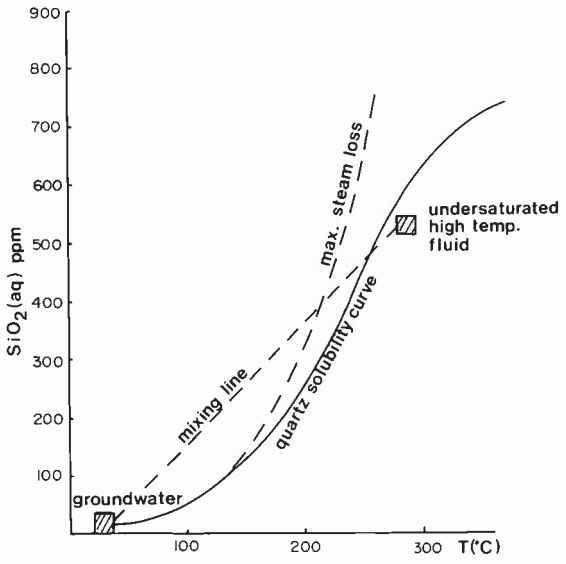

Fig. 6. Silica solubility vs. temperature (from Truesdell and Fournier, 1977). If a high-temperature silica-saturated fluid were mixed with a low-temperature silica-saturated fluid, the resulting fluid would be silica supersaturated.

and Barren Beds where reaction with carbonaceous silty limestones raised pH and lowered f_{O_2} of the fluid. Continued reaction with the silty limestones produced totally decarbonated sericite–kaolinite-rich rocks, consistent with the field observations, phyllosilicate mineralogy and bulk chemical relationships presented in this paper.

The solubility of Au and the role of gold chloride and sulfide complexes in Au transportation and deposition are controversial [see reviews and accompanying references in Seward (1983) and Henley and Ellis (1983)]. This controversy is particularly difficult to resolve for Carlin-type deposits in which the physical association of the Au is not exactly known. Most authors consider Au to have a +1 valence under hypogene conditions and to be transported by either the $AuCl_2^-$ complex or one of a variety of gold sulfide or bisulfide complexes. Equilibrium constants provided by different investigators are variable, but all generally agree that $AuCl_2^-$ predominates in acidic oxidized fluid and bisulfide complexes are characteristic of reduced fluids.

The chemical environment for deposition of Au accompanied by argillic facies and vein minerals is shown in Fig. 5. Also shown are gold chloride and bisulfide concentrations in Mercur hydrothermal solutions. The Mercur chemical environment is near a Au solubility minimum. Au would be more soluble (chloride complex) in solutions that were more oxidizing or more acid and more soluble (bisulfide complex) in solutions that were less oxidized. The mineralogical characteristics of the Mercur ore do not resolve the problem of which complex is responsible for Au transport, but oxidation, reduction, cooling and mixing of hydrothermal solutions are all involved in various parts of the deposit. The Silver Chert results from cooling or fluid mixing, but oxidation of Au thio-complexes in the Silver Chert horizon would concentrate Au and As mineralization there rather than in the overlying Mercur Beds. Silica encapsulation of the Au as a result of contemporaneous precipitation with silica might also be expected, contrary to what is observed. A possible explanation may be that following jasperoid formation, unreacted H_2S-bearing fluids passed through the relatively inert jasperoid into the overlying rocks. This is consistent with petrographic observation of reduced organic-rich fluids overprinting early-oxidized decarbonated silty limestones. Precipitation of Au could then result from destabilization of the gold bisulfide complex by organic matter and cooling.

Acknowledgements

A Chevron Graduate Fellowship in Geology provided financial support for the senior author. Additional funding was given by Getty Mining Company. Special thanks are due to R. Blair and W. Tafuri for making their accumulated knowledge of Mercur available and the geologic staff at Mercur – L. Kornze, M. Bryant, T. Faddies, S. Johnson and J. Goodwin – for helping us during our visits to the mine. Microprobe time and manuscript preparation aid was provided by the Department of Geological and Geophysical Sciences, Princeton University. Reviews by J. Bowman, G. Harper, D. Crerar, P. Vikre, T. Cerling and R. Loucks improved the manuscript.

References

Aagaard, P. and Helgeson, H.C., 1983. Activity composition relations silicates and aqueous solutions, II. Chemical and thermodynamic consequences of ideal mixing on homological sites in montmorillonites, illites and mixed layer clays. Clays Clay Miner., 31: 207–217.

Albee, A.L. and Ray, L., 1970. Correction factors for electron probe microanalysis of silicates, oxides, carbonates, phosphates and sulphates. Anal. Chem., 42: 1408–1414.

Bagby, W.C. and Berger, B.R., 1985. Geologic characteristics of sediment-hosted, disseminated, precious-metal deposits in the western United States. In: B.R. Berger and P.M. Bethke (Editors), Geology and Geochemistry of Epithermal Systems. Soc. Econ. Geol., Rev. Econ. Geol., 2: 169–202.

Barnes, H.L., 1979. Solubilities of ore minerals. In: H.L. Barnes (Editor), Geochemistry of Hydrothermal Ore

Deposits. Wiley, New York, N.Y., 2nd ed., pp. 404–460.
Bodnar, R.J. and Bethke, P.M., 1984. Systematics of stretching of fluid inclusions, I. Fluorite and sphalerite at 1 atmosphere confining pressure. Econ. Geol., 79: 141–161.
Bodnar, R.J., Reynolds, T.J. and Kuehn, C.A., 1985. Fluid inclusion systematics in epithermal systems. In: B.R. Berger and P.M. Bethke (Editors), Geology and Geochemistry of Epithermal Systems. Soc. Econ. Geol., Rev. Econ. Geol., 2: 73–97.
Butler, B.S., Loughlin, G.F., Heikes, V.C. et al., 1920. The ore deposits of Utah. U.S. Geol. Surv., Prof. Pap. No. 111, 672 pp.
Collins, P.L.F., 1979. Gas hydrates in CO_2-bearing fluid inclusions and the use of freezing data for estimation of salinity. Econ. Geol., 74: 1435–1444.
Craig, J.R. and Barton, Jr., P.B., 1973. Thermochemical approximations for sulfosalts. Econ. Geol., 68: 493–506.
Crawford, M.L., 1981. Phase equilibria in aqueous fluid inclusions. In: L.S. Hollister and M.L. Crawford (Editors), Fluid Inclusions: Applications to Petrology. Mineral. Assoc. Can., Short Course, pp. 75–97.
Drummond, S.E., 1981. Boiling and mixing of hydrothermal fluids: Chemical effects on mineral precipitation. Ph.D. Thesis, Pennsylvania State University, University Park, Pa., 380 pp.
El-Dahhar, M.A. and Barnes, H.L., 1979. Kinetics of marcasite formation. Am. Geophys. Union Trans., 60: 421 (abstract).
Ellis, A.J., 1979. Explored geothermal systems. In: H.L. Barnes (Editor), Geochemistry of Hydrothermal Ore Deposits. Wiley, New York, N.Y., 2nd ed., pp. 632–683.
Fournier, R.O. and Truesdell, A.H., 1973. An empirical Na-K-Ca geothermometer for natural waters. Geochim. Cosmochim. Acta, 37: 1255–1275.
Gaudette, H.E., Flight, W.R., Loner, L. and Folger, D.W., 1974. An inexpensive method for determination of organic carbon in recent sediments. J. Sediment. Petrol., 44: 249–253.
Gilluly, J., 1932. Geology and ore deposits of the Stockton and Fairfield quadrangles, Utah. U.S. Geol. Surv., Prof. Pap. No. 173, 171 pp.
Haas, J.L., 1971. The effect of salinity on the maximum gradient of a hydrostatic system at hydrostatic pressure. Econ. Geol., 66: 940–946.
Hedenquist, J.W., 1986. Precious metal vein systems in the National District, Humboldt County, Nevada – a discussion. Econ. Geol., 81: 1020–1022.
Hedenquist, J.W. and Henley, R.W., 1985. The importance of CO_2 freezing point measurements of fluid inclusions: evidence from active geothermal systems and implications for epithermal ore deposits. Econ. Geol., 80: 1379–1406.
Helgeson, H.C., 1969. Thermodynamics of hydrothermal systems at elevated temperatures and pressures. Am. J. Sci., 267: 729–804.
Helgeson, H.C., Delany, J.M., Nesbitt, M.W. and Bird, D.K., 1978. Summary and critique of the thermodynamic properties of rock-forming minerals. Am. J. Sci., 276: 1–278.
Henley, R.W. and Ellis, A.J., 1983. Geothermal systems ancient and modern: a geochemical review. Earth-Sci. Rev., 19: 1–50.
Hollister, L.S., Crisp, J.A., Kulick, C.G., Maze, W. and Sisson, V.B., 1984. Quantitative energy dispersive analysis of rock-forming silicates. Proc. 19th Annu. Microbeam Anal. Soc. Meet., pp. 143–144.
Hutchinson, C.S., 1974. Laboratory Handbook of Petrographic Techniques. Wiley, New York, N.Y., 527 pp.
MacDonald, A.J. and Spooner, E.T.C., 1981. Calibration of a Linkan TH *600* programmable heating-cooling stage for microthermetric examination of fluid inclusions. Econ. Geol., 76: 1248–1258.
McDowell, S.D. and Elders, W.A., 1980. Layer silicate minerals in borehole Elmore no. *1*, Salton Sea geothermal field, California, U.S.A. Contrib. Mineral. Petrol., 74: 293–310.
Murowchick, J.B. and Barnes, H.L., 1986. Marcasite precipitation from hydrothermal solutions. Geochim. Cosmochim. Acta, 50: 2615–2629.
Parry, W.T., Ballantyne, J.M. and Jacobs, D.C., 1984. Geochemistry of hydrothermal sericite from Roosevelt hot springs and the Tintic and Santa Rita porphyry copper systems. Econ. Geol., 79: 72–86.
Potter II, R.W., Clynne, M.A. and Brown, D.L., 1978. Freezing point depression of aqueous sodium chloride solutions: Econ. Geol., 73: 284–285.
Radtke, A.S., 1985. Geology of the Carlin gold deposit. U.S. Geol. Surv., Prof. Pap. No. 1267, 124 pp.
Radtke, A.S., Rye, R.O. and Dickson, F.W., 1980. Geology and stable isotope studies of the Carlin gold deposit, Nevada. Econ. Geol., 75: 642–672.
Reed, M.H., 1982. Calculation of multicomponent chemical equilibria and reaction processes in systems involving minerals, gases, and an aqueous phase. Geochim. Cosmochim. Acta, 46: 513–528.
Rising, B.A., 1973. Phase relations among pyrite, marcasite, and pyrrhotite below 300°C. Ph.D. Thesis, Pennsylvania State University, University Park, Pa. (unpublished).
Roedder, E., 1979. Fluid inclusions as samples of ore fluids. In: H.L. Barnes (Editor), Geochemistry of Hydrothermal Ore Deposits. Wiley, New York, N.Y., 2nd ed., pp. 684–737.
Rybach, L. and Muffler, L.J.P., 1981. Geothermal Systems – Principles and Case Histories. Wiley, New York, N.Y., 359 pp.
Seward, T.M., 1973. Thio-complexes and the transport of gold in hydrothermal ore solutions. Geochim. Cosmochim. Acta, 37: 379–399.
Seward, T.M., 1983. The transport and deposition of gold in hydrothermal systems. In: R.P. Foster (Editor), Gold

'82: The Geology, Geochemistry, and Genesis of Gold Deposits. Geol. Soc. Zimbabwe, Spec. Publ., 1: 165–181.

Spurr, J.E., 1895. Economic geology of the Mercur mining district, Utah. U.S. Geol. Survey 16th Annu. Rep., Part 2, pp. 374–376.

Truesdell, A.H. and Fournier, F.O., 1977. Procedures for estimating temperature of a hot-water component in a mixed water by using a plot of dissolved silica versus enthalpy. J. Res. U.S. Geol. Surv., 5(1): 49–52.

Vikre, P.G., 1985. Precious metal vein systems in the National District, Humboldt County, Nevada. Econ. Geol., 80: 360–393.

Vikre, P.G., 1986. Precious metal vein systems in the National District, Humboldt County, Nevada – a reply. Econ. Geol., 81: 1023–1024.

Weaver, C.E. and Pollard, L.D., 1973. The Chemistry of Clay Minerals. Elsevier, Amsterdam, 213 pp.

Wood, S.A., 1985. Some aspects of the hydrothermal geochemistry of ore forming solutions. Ph.D. Thesis, Princeton University, Princeton, N.J. (unpublished).

Wood, S.A., Crerar, D.A., Brantley, S.L. and Borcsik, M.P., 1985. Mean molal activity coefficients of alkali halides and related electrolytes in hydrothermal solutions. Am. J. Sci., 285: 668–705.